Ferrocene Linked to PtL_2 Fragments ($L_2 = Cl_2$, Fumaronitrile, 3,6-Di-*tert*-butylcatecholato): A Spectroscopic and Theoretical Investigation of Redox Behavior and Charge Distributions†

Katja Heinze* and Sven Reinhardt

Department of Inorganic Chemistry, University of Heidelberg, Im Neuenheimer Feld 270, D-69120 Heidelberg, Germany

Received June 14, 2007

The optical and redox properties of a ferrocene-appended diimine ligand (**1**) and its PtL_2 complexes [$L_2 = Cl_2$ (**2**), fumaronitrile (**3**), 3,6-di-*tert*-butylcatecholato (**4**)] are reported. The chromophores are characterized by NMR, UV/vis, and IR spectroscopy as well as cyclic voltammetry. Preparative oxidations to radical cations using "Magic Blue" $[N(p\text{-}C_6H_4Br)_3][SbCl_6]$ or silver triflate in conjunction with UV/vis, NMR, and EPR spectroscopy were used to probe the chloride-dependent redox chemistry of ligand **1** and platinum complexes **2**−**4**. Density functional calculations were employed to corroborate geometric and electronic descriptions of **1**−**4** and their oxidized counterparts.

Introduction

Square planar platinum(II) complexes have found widespread applications as cytostatic drugs,[1−4] as potential photocatalysts,[5−8] as artificial photosynthetic devices,[9] as NLO materials,[10,11] as electrophosphorescent dopants in OLEDs,[12−14] and as sensitizers in dye-sensitized solar cells.[15] In many cases chelating diimine ligands serve as ancilliary ligands while the remaining coligands tune the properties of the resulting complex; e.g., Pt(dithiolate)(diimine) complexes are luminescent while Pt(diolate)(diimine) and Pt(catecholate)(diimine) complexes usually are nonluminescent at ambient temperature. On the other hand, the steric and electronic specifications of diimine ligands often determine the catalytic properties of (diimine)ML_n complexes (M = Ni, Pd, etc.).[16−18]

Ferrocenes have been appended to diimine ligands and to coligands to tune the catalytic performance of homogeneous catalysts and to install redox-switchable tags onto catalysts to simplify catalyst recovery.[19−24] To fully exploit the redox properties of ferrocenes appended to transitions metal complexes for tuning catalytic and optical properties, it is essential to gain insight into the electronic situation of ferrocene appended transition metal complexes and to understand their redox behavior. Ferrocenes as electron donors have also been connected to the quinone/semiquinone/hydroquinone redox system with proton-dependent redox chemistry.[25−27] The study of such dyads has provided new insight into unusual charge distributions (valence tautomerism, bistability), proton-coupled electron-transfer reactions, and the role of hydrogen bonding in excited charge-separated states. Ligand- versus metal-centered redox chemistry of transition metal complexes with catecholato and/

* To whom correspondence should be addressed. Fax: int + 49 6221 548587. Tel.: int + 49 6221 545707. E-mail: katja.heinze@urz.uni-heidelberg.de.

† This article is dedicated to Professor Gottfried Huttner on the occasion of his 70th birthday.

(1) Wong, E.; Giandomenico, C. M. *Chem. Rev.* **1999**, *99*, 2451−2466.
(2) Jamieson, E. R.; Lippard, S. J. *Chem. Rev.* **1999**, *99*, 2467−2498.
(3) Reedijk, J. *Chem. Rev.* **1999**, *99*, 2499−2510.
(4) Conrad, M. L.; Enman, J. E.; Scales, S. J.; Zhang, H.; Vogels, C. M.; Saleh, M. T.; Decken, A.; Westcott, S. A. *Inorg. Chim. Acta* **2005**, *358*, 63−69.
(5) Kumar, L.; Puthraya, K. H.; Srivastava, T. S. *Inorg. Chim. Acta* **1984**, *86*, 173−178.
(6) Connick, W. B.; Gray, H. B. *J. Am. Chem. Soc.* **1997**, *119*, 11620−11627.
(7) Zhang, Y.; Ley, K. D.; Schanze, K. S. *Inorg. Chem.* **1996**, *35*, 7102−7110.
(8) Chassot, L.; von Zelewsky, A.; Sandrini, D.; Maestri, M.; Balzani, V. *J. Am. Chem. Soc.* **1986**, *108*, 6084−6085.
(9) Hissler, M.; McGarrah, J. E.; Connick, W. B.; Geiger, D. K.; Cummings, S. D.; Eisenberg, R. *Coord. Chem. Rev.* **2000**, *208*, 115−137.
(10) Base, K.; Tierney, M. T.; Fort, A.; Muller, J.; Grinstaff, M. W. *Inorg. Chem.* **1999**, *38*, 287−289.
(11) Cummings, S. D.; Cheng, L.-T.; Eisenberg, R. *Chem. Mater.* **1997**, *9*, 440−450.
(12) Lin, Y.-Y.; Chan, S.-C.; Chan, M. C. W.; Hou, Y.-J.; Zhu, N.; Che, C.-M.; Liu, Y.; Wang, Y. *Chem.−Eur. J.* **2003**, *9*, 1263−1272.
(13) Chan, S.-C.; Chan, M. C. W.; Wang, Y.; Che, C.-M.; Cheung, K.-K.; Zhu, N. *Chem.−Eur. J.* **2001**, *7*, 4180−4190.
(14) Furuta, P. T.; Deng, L.; Garon, S.; Thompson, M. E.; Fréchet, J. M. J. *J. Am. Chem. Soc.* **2004**, *126*, 15388−15389.
(15) Geary, E. A. M.; Yellowlees, L. J.; Jack, L. A.; Oswald, I. D. H.; Parsons, S.; Hirata, N.; Durrant, J. R.; Robertson, N. *Inorg. Chem.* **2005**, *44*, 242−250.
(16) Benito, J. M.; de Jesus, E.; de la Mata, F. J.; Flores, J. C.; Gomez, R. *Organometallics* **2006**, *25*, 3045−3055.
(17) Benito, J. M.; de Jesus, E.; de la Mata, F. J.; Flores, J. C.; Gomez, R.; Gomez-Sal, P. *Organometallics* **2006**, *25*, 3876−3887.
(18) Gibson, V. C.; Halliwell, C. M.; Long, N. J.; Oxford, P. J.; Smith, A. M.; White, A. J. P.; Williams, D. J. *Dalton Trans.* **2003**, 918−926.
(19) Siemeling, U.; Bausch, K. *Inorg. Chim. Acta* **2005**, *358*, 2146−2148.
(20) Siemeling, U. *Z. Anorg. Allg. Chem.* **2005**, *631*, 2957−2966.
(21) Siemeling, U.; Bausch, K.; Fink, H.; Bruhn, C.; Baldus, M.; Angerstein, B.; Plessow, R.; Brockhinke, A. *Dalton Trans.* **2005**, 2365−2374.
(22) Sprigings, T. G.; Hall, C. D. *Organometallics* **2001**, *20*, 2560−2564.
(23) Bildstein, B.; Malaun, M.; Kopacka, H.; Wurst, K.; Mitterböck, M.; Ongania, K.-H.; Opromolla, G.; Zanello, P. *Organometallics* **1999**, *18*, 4325−4336.
(24) Süssner, M.; Plenio, H. *Angew. Chem., Int. Ed.* **2005**, *44*, 6885−6888.
(25) Colbran, S. B.; Lee, S. T.; Lonnon, D. G.; Maharaj, F. J. D.; McDonagh, A. M.; Walker, K. A.; Young, R. D. *Organometallics* **2006**, *25*, 2216−2224.
(26) Fukuzumi, S.; Yoshida, Y.; Okamoto, K.; Imahori, H.; Araki, Y.; Ito, O. *J. Am. Chem. Soc.* **2002**, *124*, 6794−6795.
(27) Murata, M.; Yamada, M.; Fujita, T.; Kojima, K.; Kurihara, M.; Kubo, K.; Kobayashi, Y.; Nishihara, H. *J. Am. Chem. Soc.* **2001**, *123*, 12903−12904.

10.1021/om700585v CCC: $37.00
Publication on Web 09/28/2007

Scheme 1. Reactions of 1[a]

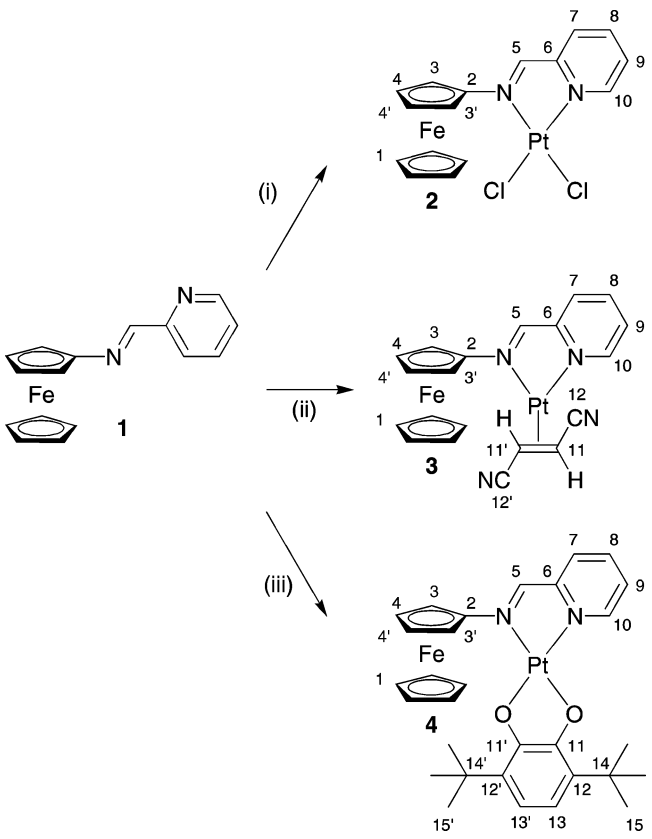

[a] Key: (i) $PtCl_2(dmso)_2$; (ii) $Pt(nb)_3$, fumaronitrile; (iii) $Pt(nb)_3$, 3,6-di-*tert*-butyl-1,2-benzoquinone.

or *o*-semiquinonato ligands[28] has been of considerable debate during the last decades and has been recently systematically addressed by Wieghardt and co-workers for the Ni, Pd, and Pt triad.[29−31]

Herein we present a study on the electronic interaction between ferrocene and PtL_2 connected by a diimine chelate with platinum in the formal oxidation states of zero and +II and the coligands varying among chloride, fumaronitrile, and a potentially noninnocent catecholato/*o*-semiquinonato/*o*-quinonato coligand. The electronic structure of oxidized species is probed by electrochemical measurements and preparative oxidation with "Magic Blue" $[N(p\text{-}C_6H_4Br)_3][SbCl_6]$ or silver triflate and subsequent UV/vis, NMR, and EPR spectroscopic analyses. Interpretations concerning geometric and electronic situations will be aided by density functional calculations.

Results and Discussion

Synthesis and Characterization of PtL_2(Fc−N∩N′) [L_2 = Cl_2 (2), Fumaronitrile (3), 3,6-Di-*tert*-butylcatecholato (4)]. The ferrocenyl-appended diimine ligand Fc−N∩N′ (**1**) has been prepared according to the literature.[18] Dichloroplatinum(II) complex (**2**) has been obtained in 69% yield from **1** and $PtCl_2(dmso)_2$,[32] while the platinum(0) complex with fumaronitrile (**3**) is conveniently prepared from **1**, $Pt(nb)_3$ (nb = norbornene),[33] and fumaronitrile via ligand exchange in 86% isolated yield (Scheme 1). The 3,6-di-*tert*-butylcatecholato complex (**4**) is accessible from **1**, $Pt(nb)_3$, and 3,6-di-*tert*-butyl-[1,2]benzoquinone[34] by oxidative addition of the quinone to platinum(0) in 45% yield (Scheme 1). All new compounds have been characterized by one- and two-dimensional NMR spectroscopy (Tables 1 and 2), IR and UV/vis spectroscopy, high-resolution mass spectrometry, cyclic voltammetry, and elemental analyses.

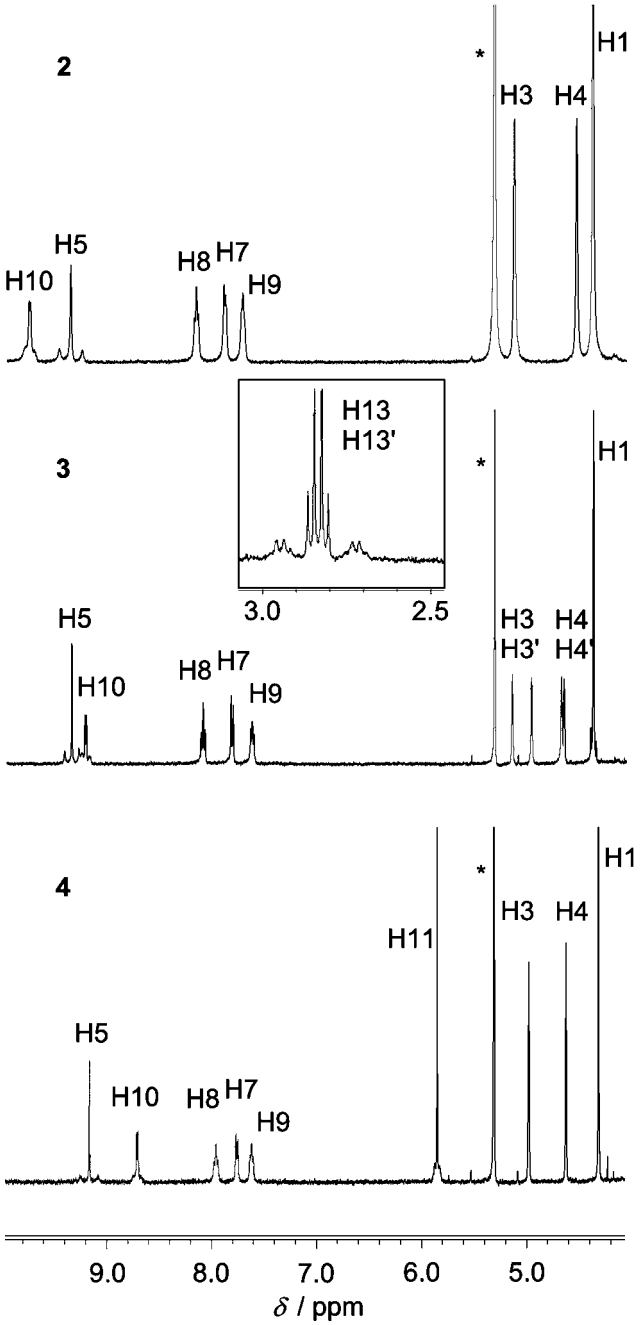

Figure 1. Partial ^1H NMR spectra of **2**−**4** in CD_2Cl_2 at 400 MHz (asterisk denotes residual $CDHCl_2$).

In the proton NMR spectra all complexes **2**−**4** display ^{195}Pt satellites for resonances of H5 and H10 with $^3J_{PtH5}$ = 88, 54, and 69 Hz and $^3J_{PtH10}$ = 37, 27, and 31 Hz, respectively (Figure

(28) Pierpont, C. G.; Lange, C. W. *Prog. Inorg. Chem.* **1994**, *41*, 331−442.
(29) Ghosh, P.; Begum, A.; Herebian, D.; Bothe, E.; Hildenbrand, K.; Weyhermüller, T.; Wieghardt, K. *Angew. Chem., Int. Ed.* **2003**, *42*, 563−567.
(30) Herebian, D.; Bothe, E.; Neese, F.; Weyhermüller, T.; Wieghardt, K. *J. Am. Chem. Soc.* **2003**, *125*, 9116−9128.
(31) Bachler, V.; Olbrich, G.; Neese, F.; Wieghardt, K. *Inorg. Chem.* **2002**, *41*, 4179−4193.
(32) Romeo, R.; Scolaro, L. M. *Inorg. Synth.* **1998**, *32*, 153−158.
(33) Crascall, L. E.; Spencer, J. L. *Inorg. Synth.* **1990**, *28*, 126−132.
(34) Paquette, L. A.; Hefferon, G. J.; Samodral, R.; Hanzawa, Y. *J. Org. Chem.* **1983**, *48*, 1262−1266.

Table 1. ^{1}H NMR Data for 2−4 in CD_2Cl_2

proton	2	3	4
H1	4.37 (s, 5H)	4.37 (s, 5H)	4.32 (s, 5H)
H3/H3	5.12 (s, 2H)	5.14 (pt, 1H)/4.96 (pt, 1H)	4.98 (pt, 2H)
H4/H4	4.53 (s, 2H)	4.68 (m, 1H)/4.65 (m, 1H)	4.63 (pt, 2H)
H5	9.35 (s, 1H, $^3J_{PtH}$ = 88 Hz)	9.34 (s, $^3J_{PtH}$ = 54 Hz, 1H)	9.16 (s, $^3J_{PtH}$ = 69 Hz, 1H)
H7	7.88 (d, $^3J_{HH}$ = 7.1 Hz, 1H)	7.81 (d, $^3J_{HH}$ = 7.9 Hz, 1H)	7.76 (d, $^3J_{HH}$ = 7.0 Hz, 1H)
H8	8.15 (pt, 1H)	8.09 (pt, 1H)	7.96 (pt, 1H)
H9	7.71 (pt, 1H)	7.62 (pt, 1H)	7.62 (pt, 1H)
H10	9.74 (d, $^3J_{HH}$ = 5.6 Hz, $^3J_{PtH}$ = 37 Hz, 1H)	9.21 (d, $^3J_{HH}$ = 5.1 Hz, ^3J(PtH) = 27 Hz, 1H)	8.71 (d, $^3J_{HH}$ = 5.2 Hz, $^3J_{PtH}$ = 31 Hz, 1H)
H11/H11		2.81 (d, $^3J_{HH}$ = 7.8 Hz, $^2J_{PtH}$ = 89 Hz, 1H)/ 2.86 (d, $^3J_{HH}$ = 7.8 Hz, $^2J_{PtH}$ = 90 Hz, 1H)	
H13/H13			5.85 (s, $^5J_{PtH}$ = 19 Hz, 2H)
H15/H15			1.23 (s, 18H)

Table 2. ^{13}C NMR Data for 2−4 in CD_2Cl_2

carbon	2	3	4
C1	71.8 (s)	71.5 (s)	71.3 (s)
C2	106.6 (s)	103.2 (s)	103.3 (s)
C3/C3	68.7 (s)	67.3 (s)/66.6 (s)	67.2 (s)
C4/C4	69.3 (s)	71.4 (s)/71.0 (s)	70.7 (s)
C5	165.0 (s)	156.2 (s)	155.4 (s)
C6	157.7 (s)	156.4 (s)	157.2 (s)
C7	126.8 (s)	126.0 (s)	126.2 (s)
C8	140.0 (s)	139.4 (s)	138.4 (s)
C9	127.9 (s)	128.5 (s)	127.4 (s)
C10	150.7 (s)	154.2 (s)	148.6 (s)
C11/C11		−0.8 (s)/0.7 (s)	178.5 (s)
C12/C12			109.2 (s)
C13/C13			90.3 (s)
C14/C14			34.7 (s)
C15/C15			29.5 (s)

1). For **3** and **4** ^{195}Pt satellites are also observed for the doublets of olefin protons H11 and H11′ with $^2J_{PtH} \approx 90$ Hz (**3**) and the singlet resonance of the catecholate protons H13/H13′ with $^5J_{PtH} = 19$ Hz (**4**) (Figure 1). All Pt−H couplings have been checked by measuring proton NMR spectra at 200 and 400 MHz.

Significant differences in proton chemical shifts are observed for pyridine proton H10 and ferrocene protons H3 and H4 in **2**−**4** (Figure 1). For the olefin complex **3** the protons H3/H3′ and H4/H4′ as well as the corresponding carbon atoms C3/C3′ and C4/C4′ are diastereotopic due to the asymmetric coordination of the (*E*)-olefin relative to the Pt−N−N′ plane which renders the platinum atom chiral (Tables 1 and 2). Thus, **3** exists as an enantiomeric pair **3** and **3′** (by rotation of the ferrocenyl substituent, Scheme 2). 2D correlation and NOE spectroscopy allowed us to assign all signals in the NMR spectrum of **3** to individual protons of **3** as NOE cross-peaks are observed between H3 and H5 as well as between H3′ and H11′. Variable-temperature ^{1}H NMR spectra in [D$_6$]DMSO remain unchanged up to 90 °C except for the two doublets for H11 and H11′ which coalesce at around 90 °C (Figure 2). The spectral changes are reversible indicating no substantial degradation of the complex. Ligand dissociation up to 90 °C is negligible as all signals including platinum satellites of H5 and H10 and diasterotopic splitting of H3 and H3′ are preserved. The coalescence is attributed to beginning olefin rotation. The activation barrier for olefin rotation is estimated as $\Delta G^{\ddagger}_{rot} = 77$ kJ mol^{-1} on the basis of the equations $k_{Tc} = 2.22(\Delta\nu^2 + 6J^2)^{1/2}$ and $\Delta G^{\ddagger}_{rot} = -RT_c \ln[k_{Tc}N_A h/(RT_c)]$ and the experimental values $T_c \approx 363$ K, $\Delta\nu = 24.0$ Hz, and $J = 7.72$ Hz. The estimated rotation barrier for the fumaronitrile ligand in **3** is in a range typical for PtL$_2$(olefin) complexes.[35] Interestingly, for Pt(η^2-fn)(^{t}Bu−N∩N′) no fluxional behavior has been observed in $CDCl_3$.[36]

However, the molecular structure of Pt(η^2-fn)(^{t}Bu−N∩N′) has been determined by X-ray crystallography which allows us to compare and validate the metric data of the DFT-optimized minimum structure of **3** (Figure 3; B3LYP, LanL2DZ) with those of Pt(η^2-fn)(^{t}Bu−N∩N′).[36] The DFT calculations will be used to interpret fluxional behavior and electronic structure of the platinum complexes (vide infra). In fact, the overall geometry is well reproduced by the calculation. The calculated C═C bond length of **3** (1.500 Å) compares well with the experimental one for Pt(η^2-fn)(^{t}Bu−N∩N′) [1.43(2) Å] as do the Pt−N$_{py}$ and Pt−N$_{im}$ distances [**3**-DFT, 2.122, 2.169 Å; Pt(η^2-fn)(^{t}Bu−N∩N′), 2.105(15), 2.134(12) Å], while the Pt−C11 and Pt−C11′ distances are somewhat overestimated by the calculation employing this level of theory [**3**-DFT, 2.079, 2.099 Å; Pt(η^2-fn)(^{t}Bu−N∩N′), 2.007(15), 2.011(14) Å]. For our purpose, however, the accuracy is sufficient. Also shown in Figure 3 are selected H···H distances relevant for the interpretation of the NOE cross-peaks and the conformation in solution (vide supra). The calculated (in the gas phase) CN stretching vibrations ($\nu_{CN,asym} = 2238$ cm^{-1}, $\nu_{CN,sym} = 2232$ cm^{-1}; not scaled) are also in line with the experimental IR data (in the solid state, $\nu_{CN,asym} = 2203$ cm^{-1}, $\nu_{CN,sym} = 2195$ cm^{-1}; in CH_2Cl_2, $\nu_{CN,asym} = 2202$ cm^{-1}, $\nu_{CN,sym} = 2193$ cm^{-1}). The transition state for olefin rotation has been calculated by DFT methods to lie at 105 kJ mol^{-1} above the ground state in good agreement with the experimental value. Likewise, the barrier for rotation of the ferrocenyl substituent (Scheme 2) has been probed by DFT calculations. As expected, an asymmetric energy profile for the torsion around C5−N$_{im}$−C2−C3 is calculated with two transition states at −100 and 70° corresponding to barriers of 31 and 50 kJ mol^{-1}.

Geometries of dichloroplatinum(II) complexes with asymmetric diimine ligands have been calculated recently by DFT methods and evaluated against experimental molecular struc-

Scheme 2. Enantiomeric Pair 3 and 3′ [a]

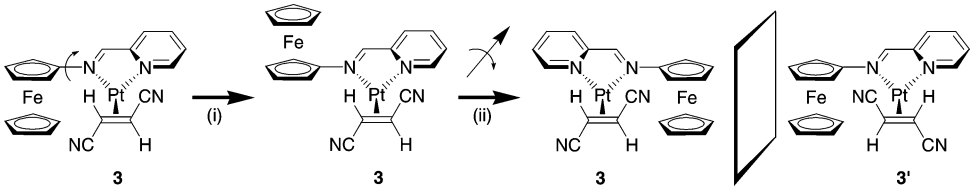

[a] Key: (i) Fc rotation; (ii) molecule rotation.

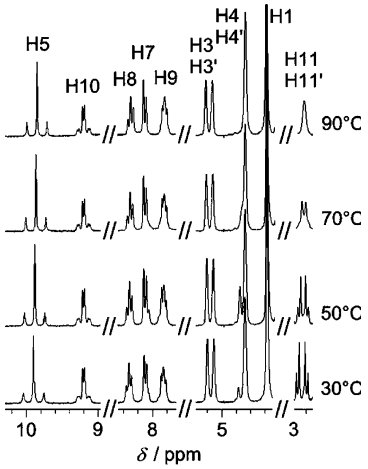

Figure 2. Variable-temperature ^{1}H NMR spectra of **3** in [D_6]-DMSO at 200 MHz.

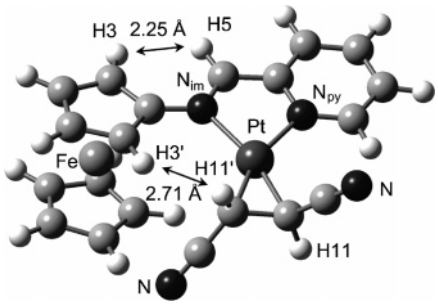

Figure 3. DFT-calculated minimum geometry of **3** with relevant H···H distances indicated.

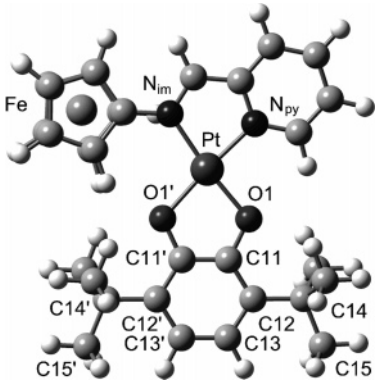

Figure 4. DFT-calculated minimum geometry of **4**.

tures.[37] So a comparison of the DFT-optimized geometry of **2** and experimental values is omitted. All values are in the expected range (Pt−N_{py} 2.043 Å; Pt−N_{im} 2.079 Å; Pt−Cl1 2.401 Å; Pt−Cl1′ 2.402 Å).

The DFT-optimized minimum geometry of **4** is depicted in Figure 4. There appears to be a negligible difference in trans influences of N_{im} and N_{py} in **4** as all Pt−O, C−O, and symmetry-related C−C distances in the catecholato ligand are very similar (Pt−O1 1.995 Å; Pt−O1′ 2.023 Å; C11−O1 1.389 Å; C11′−O1′ 1.391 Å; C11−C12 1.420 Å; C11′−C12′ 1.422 Å; C12−C13 1.408 Å; C12′−C13′ 1.408 Å). Accordingly, the protons H13 and H13′ as well as the carbon atoms C11/ C11′, C12/C12′, and C13/C13′ are magnetically indistinguishable in the NMR spectra (vide supra). The calculated C−O distances are in the typical range for coordinated catecholato ligands and justify the description of **4** as a catecholato complex.[38] The calculated Pt−N distances are the shortest in the series of complexes **2**−**4** (Pt−N_{py} 2.007 Å; Pt−N_{im} 2.048 Å), which may point to some charge delocalization in the ground state from the catecholato to the diimine ligand mediated by Pt(dπ) orbitals.

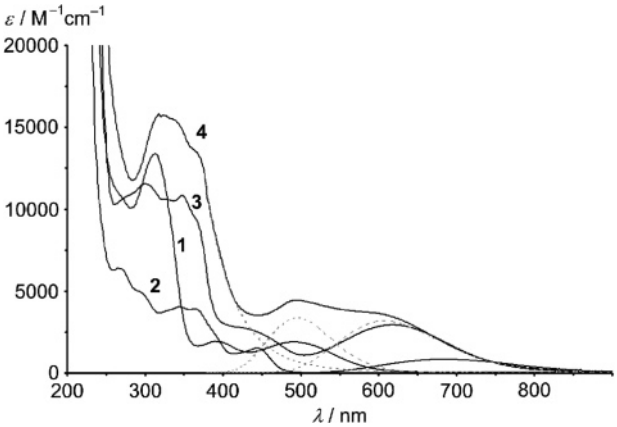

Figure 5. UV/vis absorption spectra of **1**−**4** in CH_2Cl_2 (and Gaussian deconvolution of the absorption bands of **4** in the visible region; dotted line).

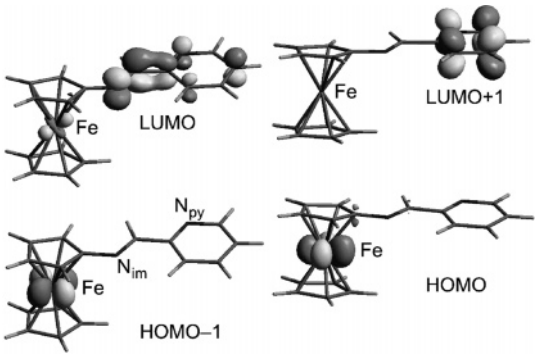

Figure 6. Ferrocene and diimine frontier Kohn−Sham orbitals of **1** (isosurfaces at 0.07 au).

Optical Spectroscopy of 1−4. All compounds **2**−**4** are deep green in the solid state and in solution, while the ferrocene-appended ligand **1** itself is orange-red with a ferrocene → diimine charge-transfer band ["e_π(HOMO-Fc)" → π*(LUMO-diimine)] at 493 nm (ϵ = 1890 M^{-1} cm^{-1}). Upon coordination of PtL_2 to the diimine, this charge-transfer band shifts to 608, 621, and 686 nm for **4**, **3**, and **2**, respectively (in CH_2Cl_2; Figure 5). These bands are negatively solvatochromic as in the more polar solvent THF they shift to lower energy by 500−1000 cm^{-1} which is indicative for different dipole moments of the ground and exited states and typical for charge-transfer transitions. If the assignment of the band as a ferrocene → diimine charge transfer is correct it is expected that the transition energy is correlated to the energy difference of the diimine LUMOs and the ferrocene HOMOs (Figure 6; B3LYP; LanL2DZ). Indeed, good correlations are observed between the energy differences of the highest occupied ferrocene-based molecular orbitals ["e_π(HOMO-Fc)"] and the two lowest empty diimine-based molecular orbitals as calculated by DFT methods (Figure 7). Thus, the observed absorption band can be ascribed to transitions from the ferrocene "e_π" orbitals to the diimine π* orbitals and the

(35) van Asselt, R.; Elsevier, C. J.; Smeets, W. J. J.; Spek, A. L. *Inorg. Chem.* **1994**, *33*, 1521−1531.
(36) Canovese, L.; Visentin, F.; Chessa, G.; Santo, C.; Uguagliati, P.; Maini, L.; Polito, M. *J. Chem. Soc., Dalton Trans.* **2002**, 3696−3704.
(37) Reinhardt, S.; Heinze, K. *Z. Anorg. Allg. Chem.* **2006**, *632*, 1465−1470.
(38) Pal, S.; Das, D.; Sinha, C.; Kennard, C. H. L. *Inorg. Chim. Acta* **2001**, *313*, 21−29.

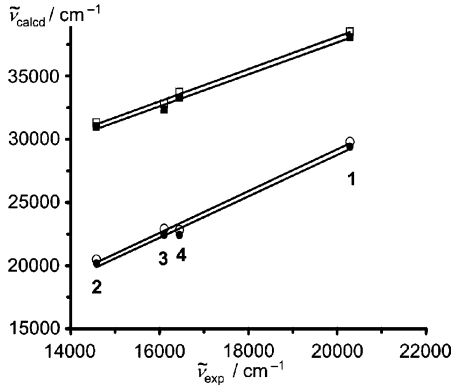

Figure 7. Correlation of the low-energy absorptions of **1**−**4** with energy differences of molecular orbitals [$Fc_{HOMO-1} \rightarrow \pi^*_{LUMO}$ (●), $Fc_{HOMO} \rightarrow \pi^*_{LUMO+1}$ (○), $Fc_{HOMO} \rightarrow \pi^*_{LUMO+1}$ (■), $Fc_{HOMO-1} \rightarrow \pi^*_{LUMO+1}$ (□)]. (The solid lines are a guide to the eye.)

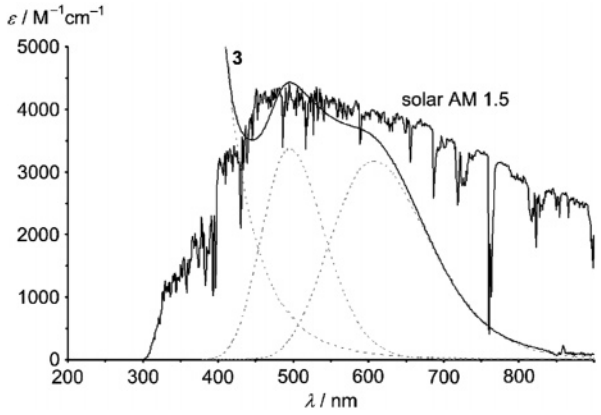

Figure 8. UV/vis absorption spectrum of **4** and a reference solar AM 1.5 spectrum.[40]

absorption energy can be tuned by coordination of PtL_2 fragments to the diimine over a range of 5700 cm^{-1} (Figure 7).

For **4** an additional absorption band is observed at 496 nm with $\epsilon = 4435$ M^{-1} cm^{-1} (obtained by spectral deconvolution). This absorption band is ascribed to a ligand-to-ligand charge transfer from the catecholate to the diimine ligand. For Pt(cat)(phen) (phen = phenanthroline, cat = catecholato) the corresponding band is found at 540 nm.[39] Thus, in **4** the dual charge transfer to the diimine results in covering the whole visible region of the solar spectral irradiance distribution with extinction coefficients of more than 1500 M^{-1} cm^{-1} (Figure 8). In this sense the two appended moieties at the diimine (Fc and catecholate) are able to harvest light energy accompanied with a charge shift to the diimine in the excited states.

Redox Chemistry of 1−4. The cyclic voltammogram of **1** in CH_2Cl_2 reveals a reversible oxidation of the ferrocene moiety at 505 mV vs SCE, which is excellent agreement with the reported value.[18] Chemical oxidation of **1** was performed using "Magic Blue" $[N(p\text{-}C_6H_4Br)_3][SbCl_6]$ with a formal redox potential of 0.7 V higher than that of ferrocene.[41] In the range 0−1 equiv of $[N(p\text{-}C_6H_4Br)_3]^{\bullet+}$ added to **1** the characteristic bands of the radical cation at 727 nm[41] are absent implying that the blue radical cation is reduced to the aromatic amine while **1** is oxidized to $\mathbf{1}^{\bullet+}$ (Figure 9). The absorption band at 493 nm decreases while a new broad band at 688 nm increases

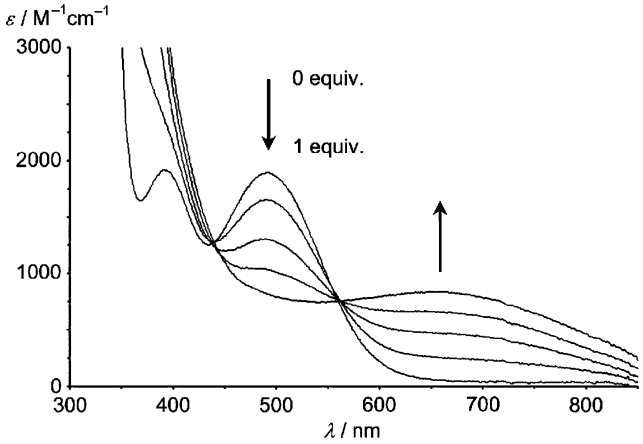

Figure 9. Titration of **1** with "Magic Blue" in CH_2Cl_2.

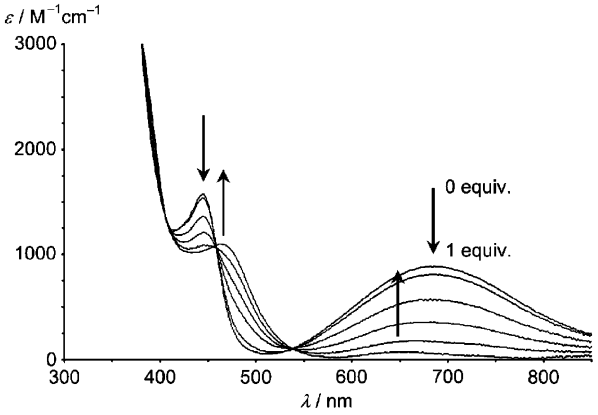

Figure 10. Titration of **2** with "Magic Blue" in CH_2Cl_2.

in intensity. The new band is tentatively assigned a ferrocenium absorption mixed with some charge-transfer character which accounts for the rather broad band. Tight isosbestic points are observed during oxidation at 438 and 561 nm suggesting a clean oxidation of **1** to $\mathbf{1}^{\bullet+}$ by $[N(p\text{-}C_6H_4Br)_3]^{\bullet+}$. Proton NMR spectra of $\mathbf{1}^{\bullet+}$ obtained by oxidation of **1** with 1 equiv of $[N(p\text{-}C_6H_4Br)_3]^{\bullet+}$ in THF show only paramagnetically broadened signals which could not be assigned with confidence.

In a CV experiment **2** displays a reversible Fc/Fc^+ oxidation at 615 mV vs SCE, which is similar to that observed for the palladium analogue $PdCl_2(Fc-N\cap N')$ (630 mV vs SCE).[18] Preparative oxidation was again accomplished using $[N(p\text{-}C_6H_4Br)_3][SbCl_6]$ in CH_2Cl_2. During oxidation the Fc → diimine CT band at 686 nm disappears as does the ferrocene band at 445 nm, while new bands at 462 and 650 nm appear (Figure 10). Again, the latter weak band is consistent with a ferrocenium moiety. Clean isosbestic points are found at 459 and 538 nm. Adding more than 1 equiv of $[N(p\text{-}C_6H_4Br)_3][SbCl_6]$ results in appearance of the typical band of the triarylamine radical cation at 727 nm[41] showing that $\mathbf{2}^{\bullet+}$ is not oxidized further by $[N(p\text{-}C_6H_4Br)_3]^{\bullet+}$. Similar to $\mathbf{1}^{\bullet+}$, ^{1}H NMR spectra of $\mathbf{2}^{\bullet+}$ obtained by oxidation of **2** with 1 equiv of $[N(p\text{-}C_6H_4Br)_3]^{\bullet+}$ in THF display only paramagnetically broadened signals which could not be assigned with confidence.

The cyclic voltammogram of the platinum(0) complex **3** displays a quasireversible oxidation at 655 mV vs SCE. However, for scan rates below 100 mV s^{-1} the reduction peak current is no more proportional to the square root of the scan rate (Figure 11). This finding suggests that a slow EC mechanism is operative giving an oxidized product which is reduced below 600 mV (Figure 11). The quasireversiblity also accounts

(39) Kamath, S. S.; Uma, V.; Srivastava, T. S. *Inorg. Chim. Acta* **1989**, *166*, 91−98.
(40) http://rredc.nrel.gov/solar/spectra/am1.5/.
(41) Connelly, N. G.; Geiger, W. E. *Chem. Rev.* **1996**, *96*, 877−910.

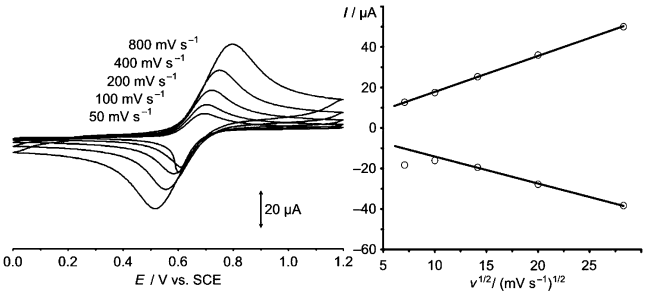

Figure 11. Cyclic voltammograms of **3** in CH_2Cl_2 at different scan rates.

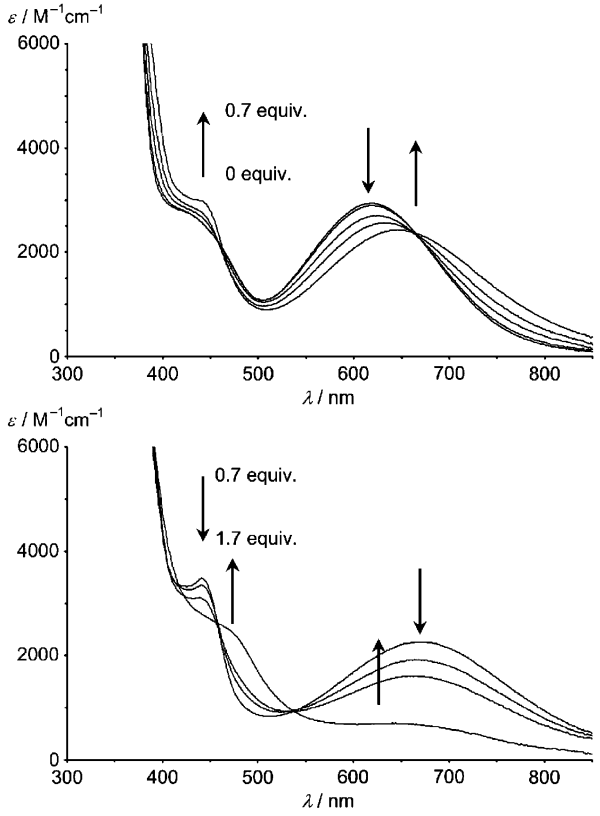

Figure 12. Titration of **3** with "Magic Blue" in CH_2Cl_2 (top, 0−0.7 equiv; bottom, 0.7−1.7 equiv).

for the high peak-to-peak separation (the peak-to-peak separation of ferrocene itself under these conditions amounts to 90 mV).

In spite of the instability of electrochemically generated $\mathbf{3}^{\bullet+}$, we were interested in the possible oxidation products. Thus, **3** was oxidized using $[N(p\text{-}C_6H_4Br)_3][SbCl_6]$ in CH_2Cl_2. The Fc → diimine CT band decreases in intensity while concomitantly a new CT band at 669 nm rises in addition to a sharp band at 441 nm (Figure 12). Isosbestic points are observed at 459 and 665 nm up to ca. 0.7 equiv of oxidant. The UV/vis spectrum after consumption of ca. 0.7 equiv of $[N(p\text{-}C_6H_4Br)_3]^{\bullet+}$ is quite similar to that of the dichloride complex **2**. In fact further oxidation with $[N(p\text{-}C_6H_4Br)_3]^{\bullet+}$ results in spectral changes also similar to those observed for the oxidation of **2** to $\mathbf{2}^{\bullet+}$, namely, reduction of the 669 and 459 nm bands, while new bands around 460 and 642 nm rise giving isosbestic points at 418 and 537 nm, respectively.

Oxidation with innocent (chloride-free) silver triflate as oxidant was performed to support the chloride-dependent oxidation with $[N(p\text{-}C_6H_4Br)_3][SbCl_6]$. With up to 1 equiv of AgOTf, the Fc → diimine CT band decreases with isosbestic points at 376, 573, and 684 nm while the second 1 equiv of AgOTf induces a bathochromic and hyperchromic shift of this band to 640 nm. This finding also suggests a more complicated reaction than just a simple oxidation of Fc to Fc^+.

To further clarify the initial oxidation events a proton NMR spectrum of **3** and 0.5 equiv of $[N(p\text{-}C_6H_4Br)_3][SbCl_6]$ was measured in CD_2Cl_2. All the products are diamagnetic with chemical shifts in the typical diamagnetic range (see above). The reduction product $N(p\text{-}C_6H_4Br)_3$ shows two doublets at $\delta = 6.93$ and 7.37 ppm with $^3J_{HH} = 8.7$ Hz. Two products each containing a Pt(Fc−N∩N′) unit are observed in the ratio 0.75:0.25 (internally referenced to the integral of the triarylamine doublets as 0.5 equiv; 6H) in addition to a singlet of free fumaronitrile at $\delta = 6.31$ ppm with an intensity corresponding to 0.75 equiv (1.5 H). The signals of the major product have striking similarity to those of $PtCl_2$(Fc−N∩N′) (**2**) in terms of chemical shifts and Pt coupling constants, while the signals of the minor product bear resemblance to those of the platinum(0) complex **3**. From a stoichiometric point of view $[N(p\text{-}C_6H_4Br)_3][SbCl_6]$ acts as a three-electron oxidant toward **3**. In this redox reaction the $SbCl_6^-$ counterion is noninnocent and acts as a source of nucleophilic chloride ions furnishing $SbCl_5$ which is itself a two-electron oxidizing agent forming $SbCl_3$.[41] The following mechanism is proposed: After one-electron transfer from 0.5 equiv of **3** to 0.5 equiv of $[N(p\text{-}C_6H_4Br)_3]^{\bullet+}$, the generated cation $\mathbf{3}^{\bullet+}$ disproportionates to 0.25 equiv of **3** and 0.25 equiv of $\mathbf{3}^{2+}$ with the latter loosing fumaronitrile (0.25 equiv). The slow disproportionation is also consistent with the electrochemical experiments. Chloride is then abstracted from the $SbCl_6^-$ anion to form 0.25 equiv of $PtCl_2$(Fc−N∩N′) (**2**) and 0.5 equiv of antimony(V) chloride. The $SbCl_5$ oxidizes another 0.5 equiv of Pt(η^2-fn)(Fc−N∩N′) (**3**) to 0.5 equiv of $PtCl_2$(Fc−N∩N′) (**2**) and fumaronitrile (0.5 equiv) giving $SbCl_3$ (0.5 equiv). The remaining 0.25 equiv of **3** is attacked by $SbCl_3$ to give a Pt^0 complex tentatively formulated as $Pt(SbCl_3)$(Fc−N∩N′).[42] The reaction of **3** with $SbCl_3$ was analyzed independently by IR and NMR spectroscopy. In the IR spectrum the characteristic asymmetric and symmetric CN absorption bands of **3** vanish and a new CN stretching absorption band appears at 2227 cm^{-1} (at the same position as a solution of fumaronitrile and $SbCl_3$ in CH_2Cl_2), and in the ^{1}H NMR spectrum of **3** and $SbCl_3$ in CD_2Cl_2 a signal for uncoordinated fumaronitrile is observed at $\delta = 6.31$. Thus, $SbCl_3$ is indeed able to displace the olefin from **3**.

The UV/vis spectroscopic results confirm this stoichiometry. Up to ca. 0.7 equiv of $[N(p\text{-}C_6H_4Br)_3][SbCl_6]$ **3** is oxidized to **2**, and further addition of $[N(p\text{-}C_6H_4Br)_3][SbCl_6]$ results in oxidation of **2** to $\mathbf{2}^{\bullet+}$. The primary reaction of **3** with $[N(p\text{-}C_6H_4Br)_3][SbCl_6]$ is summarized as follows:

$$\mathbf{3} + 2/3[N(p\text{-}C_6H_4Br)_3][SbCl_6] \rightarrow \mathbf{2} + 2/3N(p\text{-}C_6H_4Br)_3 + 2/3SbCl_3 + \text{fn} \quad (1)$$

The catecholato complex **4** displays two oxidation waves in the cyclic voltammogram at 505 and 770 mV vs SCE, the first one being quasi-reversible (Figure 13). For the comparable complexes Pt(4-*tert*-Bu-cat)(bpy) (4-*tert*-Bu-cat = 4-*tert*-butylcatecholato, bpy = 2,2′-bipyridine)[39] and Pt(3,5-dtcat)(dpphen) (3,5-dtcat = 3,5-di-*tert*-butylcatecholato, dpphen = 4,7-diphenyl-1,10-phenanthroline),[43] the catecholate oxidations are observed at 430 and 470 mV vs SCE, respectively; thus, the first oxidation of **4** is believed to be the catecholate to *o*-semiquinone

(42) Garrou, P. E.; Hartwell, G. E. *Inorg. Chem.* **1976**, *15*, 730−732.
(43) Weinstein, J. A.; Tierney, M. T.; Davies, E. S.; Base, K.; Robeiro, A. A.; Grinstaff, M. W. *Inorg. Chem.* **2006**, *45*, 4544−4555.

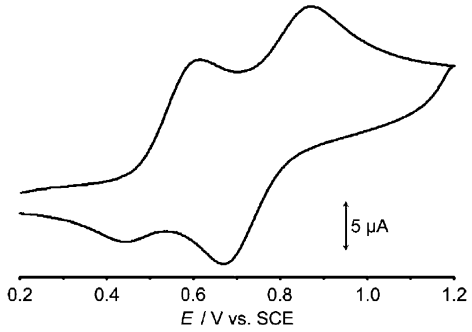

Figure 13. Cyclic voltammogram of **4** in CH_2Cl_2.

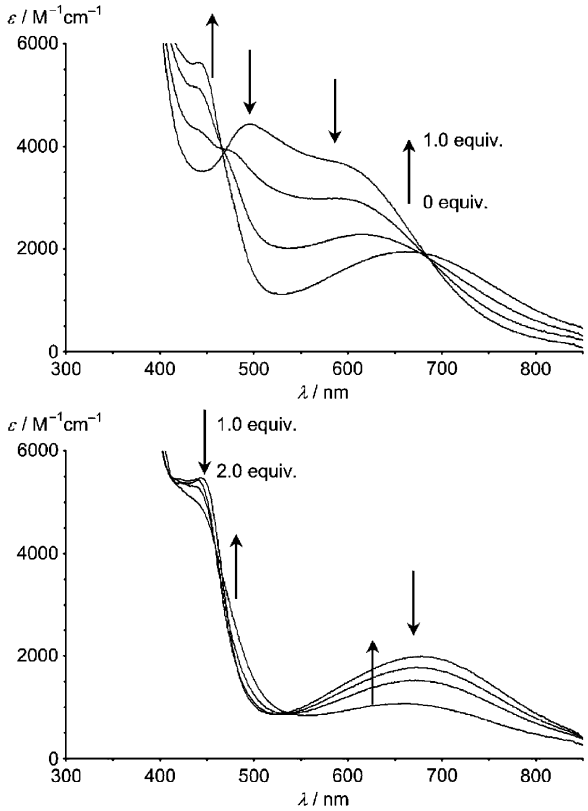

Figure 14. Titration of **4** with "Magic Blue" in CH_2Cl_2 (top, 0−1 equiv; bottom, 1−2 equiv).

oxidation and the second one the Fc/Fc^+ oxidation. To gain insight into the oxidation processes, chemical oxidation was performed with "Magic Blue" in CH_2Cl_2 and studied by UV/vis spectroscopy. Both CT bands at 496 and 608 nm lose intensity while new bands at 443 and 675 nm arise (Figure 14). Up to 1 equiv, isosbestic points are observed at 467 and 682 nm. The final spectrum bears resemblance to that of **2**. Thus the new bands are assigned ferrocene transitions and Fc → diimine CT transitions. Further addition of $[N(p\text{-}C_6H_4Br)_3][SbCl_6]$ results in spectral changes similar to those observed during oxidation of **2** to $\mathbf{2}^{\bullet+}$, namely diminishing the intensity of 443 and 675 nm bands and rise of weak bands at 475 and 660 nm.

The proton NMR spectrum of a solution of **4** and a substoichiometric amount of $[N(p\text{-}C_6H_4Br)_3][SbCl_6]$ (0.5 equiv) shows signals only in the diamagnetic region. In fact, resonances of the dichloro complex **2** (0.5 equiv) are observed with characteristic platinum coupling patterns in addition to signals corresponding to remaining **4** (0.5 equiv). Furthermore, signals for 3,6-di-*tert*-butyl-1,2-benzoquinone (3,6-^{t}Bu$_2$bq, 0.25 equiv) are found at $\delta = 6.78$ and 1.24 ppm together with signals at δ = 6.46 and 1.32 ppm (0.25 equiv) ascribed to a complex formed from 3,6-^{t}Bu$_2$cat and $SbCl_6^-$ which is tentatively formulated as Sb_2(3,6-^{t}Bu$_2$cat)Cl_8.[44,45] Thus, after one-electron transfer from the amine radical cation to give $\mathbf{4}^{\bullet+}$ the coordinated *o*-semiquinone 3,6-^{t}Bu$_2$sq is displaced by chloride ions to form **2**. The *o*-semiquinone disproportionates to the *o*-benzoquinone and the catecholate with the latter coordinating to antimony.

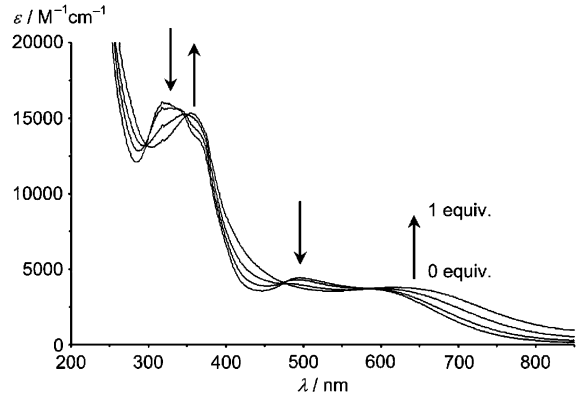

Figure 15. Titration of **4** with silver triflate in CH_2Cl_2.

The observation that 1 equiv of $[N(p\text{-}C_6H_4Br)_3][SbCl_6]$/**4** is sufficient for the primary redox process is consistent with the results from the UV/vis data. Thus, $[N(p\text{-}C_6H_4Br)_3][SbCl_6]$ acts as a one-electron oxidant and chloride donor toward **4**. The overall stoichiometric reaction is summarized as follows:

$$\mathbf{4} + [N(p\text{-}C_6H_4Br)_3][SbCl_6] \rightarrow \mathbf{2} + N(p\text{-}C_6H_4Br)_3 + 1/2Sb_2(3,6\text{-}{}^tBu_2cat)Cl_8 + (1/2)3,6\text{-}{}^tBu_2bq \quad (2)$$

From the cyclic voltammogram of **4**, it is expected that the first (quasireversible) oxidation is localized on the catecholato ligand to give the *o*-semiquinone while the second oxidation corresponds to the ferrocene/ferrocenium oxidation. Using the innocent (chloride-free) one-electron oxidant silver triflate, **4** is cleanly oxidized to $\mathbf{4}^{\bullet+}$ in CH_2Cl_2. During oxidation the catecholate to diimine CT band at 496 nm loses intensity while the ferrocene to diimine CT band shifts from 608 to 617 nm (Figure 15). Isosbestic points are observed at 297, 355, 475, and 583 nm. Interestingly, for the related electrochemically generated complex $[Pt(3,5\text{-dtsq})(dpphen)]^{\bullet+}$ (3,5-dtsq = 3,5-di-*tert*-butylsemiquionato, dpphen = 4,7-diphenyl-1,10-phenanthroline) with a symmetric diimine ligand and an asymmetrically substituted *o*-semiquinone ligand, a new band around 478 nm ($\epsilon \approx 10\,000$ M^{-1} cm^{-1}) is observed which has been assigned $d_\pi(Pt)-\pi^*$(*o*-semiquinone) MLCT character.[43] For $\mathbf{4}^{\bullet+}$ such a discrete band is not observed, but it might be hidden under the intense absorption band at 346 nm.

The nature of the radical cation $\mathbf{4}^{\bullet+}$ was probed by EPR spectroscopy. The X-band EPR spectrum (Figure 16) of $\mathbf{4}^{\bullet+}$ at room temperature is a superposition of two spectra corresponding to species with a platinum nucleus with $I = 0$ (66.3%) and $I = 1/2$ (33.7%, ^{195}Pt). The spectra show typical π radical signals with *g* around 2.0 which could be simulated using $g_{iso} = 2.0030$, $A_{iso}(^{195}Pt) = 24.2$ G, $A_{iso}(^1H) = 4.25$ G, $A_{iso}(^1H) = 4.55$ G, and $A_{iso}(2 \times {}^{14}N) = 1.75$ G (line width 1.55 G). The unpaired electron in $\mathbf{4}^{\bullet+}$ couples to two different hydrogen nuclei (H13, H13′) of the *o*-semiquinonato ligand comparable to the coupling found in the 1,4-benzosemiquinone-appended ferrocene deriva-

(44) Malhotra, K. C.; Mahajan, V. P., Miss; Chaudhry, S. C. *Curr. Sci.* **1981**, *50*, 89−91.
(45) Tian, Z.; Tuck, D. G. *J. Chem. Soc., Dalton Trans.* **1993**, 1381−1385.

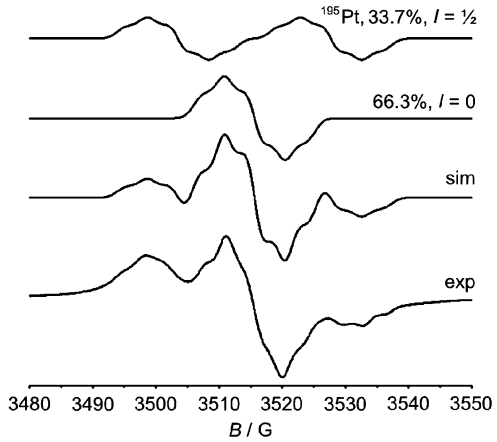

Figure 16. X-band EPR spectrum of $\mathbf{4}^{\bullet+}$ at 300 K in CH_2Cl_2 (bottom) and simulation (top). Conditions: frequency, 9.855 78 GHz; power, 19.92 mW; modulation amplitude, 10 G.

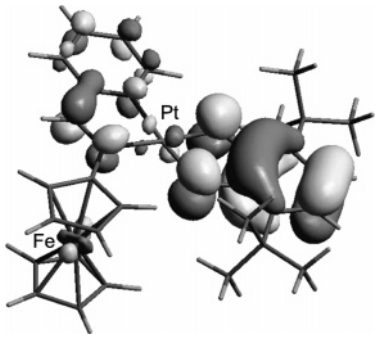

Figure 17. Singly occupied molecular Kohn−Sham orbital of $\mathbf{4}^{\bullet+}$ (isosurface at 0.03 au).

tive $[Fc-C_6H_4NHCOC_6H_3O_2]^{\bullet-}$ ($A_{iso}(^1H)$ = 4.60, 2.05, 1.75 G).[26] For Pd(3,6-dtsq)(bpy) (3,6-dtsq = 3,6-di-*tert*-butylsemiquinonato), coupling of the unpaired electron to two equivalent protons of the *o*-semiquinone has been reported with $A_{iso}(2 \times {}^1H)$ = 3.5 G[29] while for Ni(3,5-dtsq)($PyBz_2$) ($PyBz_2$ = *N*,*N*-bis(benzyl)-*N*-[(2-pyridyl)methyl]amine) coupling to one proton is observed with $A_{iso}(^1H)$ = 3.8 G.[46]

The hyperfine couplings to platinum and nitrogen show that the unpaired electron also interacts with the platinum as well as with the diimine nitrogen nuclei. The coupling constant to platinum is of somewhat lower magnitude than that found for $[Pt(3,5\text{-dtsq})(dpphen)]^{\bullet+}$ [$A_{xx}(^{195}Pt)$ = 52 G, $A_{yy}(^{195}Pt)$ = 33 G, $A_{zz}(^{195}Pt)$ = 21 G; $A_{iso}(^{195}Pt)$ = 35 G)].[43] These coupling constants have been interpreted as indicative of a SOMO mainly localized on the *o*-semiquinone with partial metal character which thus also applies for $\mathbf{4}^{\bullet+}$. In addition the unpaired electron in $\mathbf{4}^{\bullet+}$ couples with the two nitrogen nuclei of the diimine ligand providing evidence for some delocalization of the unpaired electron onto the diimine ligand via the platinum atom.

Indeed, DFT calculations support the interpretations on the basis of experimental data. The HOMO of **4** (and the SOMO of $\mathbf{4}^{\bullet+}$) is mainly localized on the catecholato/*o*-semiquinonato ligand with contributions of platinum, the diimine ligand, and iron (Figure 17). Natural charge analyses of neutral and oxidized species reveal that the first oxidation of **4** takes place on the catecholato ligand—in contrast to complex **2** and ligand **1** which display a ferrocene-based oxidation. Table 3 summarizes the natural charges of selected fragments of $\mathbf{1}/\mathbf{1}^{\bullet+}$, $\mathbf{2}/\mathbf{2}^{\bullet+}$, $\mathbf{3}/\mathbf{3}^{\bullet+}$, and $\mathbf{4}/\mathbf{4}^{\bullet+}/\mathbf{4}^{2+}$. In all cases the platinum retains its charge; i.e., it is hardly affected by the initial oxidation process.

(46) Ohtsu, H.; Tanaka, K. *Chem. Eur. J.* **2005**, *11*, 3420−3426.

Table 3. DFT-Calculated Natural Charges of Selected Fragments

complex	$FeCp_2$	diimine	L_2	Pt	Fe
1	0.21	−0.21			0.24
$\mathbf{1}^{\bullet+}$	1.02	−0.02			0.68
2	0.34	−0.05	−1.01	0.72	0.25
$\mathbf{2}^{\bullet+}$	1.15	0.08	−0.95	0.73	0.71
3	0.33	−0.13	−0.71	0.51	0.24
$\mathbf{3}^{\bullet+}$	1.15	0.00	−0.65	0.50	0.69
4	0.31	−0.21	−1.08	0.97	0.25
$\mathbf{4}^{\bullet+}$	0.43	0.06	−0.44	0.95	0.26
$\mathbf{4}^{2+}$(triplet)	1.23	0.20	−0.36	0.94	0.73
$\mathbf{4}^{2+}$(singlet)	0.70	0.19	0.14	0.97	0.37

EPR hyperfine coupling parameters were calculated by a single-point DFT calculation using the EPR-II basis set of Barone for H, C, N, and O,[47] the 6-31+g(d,p) for Fe, and the WTBS basis set[48−50] for Pt on the B3LYP/LanL2DZ-optimized geometry. Hyperfine splittings (hfc) to H13 and H13′ were estimated as 3.6 and 3.3 G, respectively, in reasonable good agreement with the experimental values while coupling to ^{14}N and ^{195}Pt is somewhat underestimated (0.36, 0.42, and 15 G, respectively). The latter is probably due to the employed nonoptimized basis set for platinum.[51] However, delocalization of spin density toward platinum and the diimine moiety is supported by the calculations.

In frozen glass matrix, $\mathbf{4}^{\bullet+}$ is EPR-silent precluding observation of individual components of **g** and **A** tensors, while on warming, the isotropic spectrum is recovered. This finding is probably due to aggregation/spin pairing in the solid matrix which has been observed previously in the crystal structure of PdL_2(bpy) (L_2 = *N*-phenyl-*o*-iminobenzosemiquinonato).[29]

Conclusion

In this study of ferrocene-appended $Pt(L_2)$(diimine) complexes with L_2 = Cl_2 (**2**), fumaronitrile (**3**), and 3,6-di-*tert*-butylcatecholato (**4**), the presence of a ferrocene moiety induces solvatochromic ferrocene to diimine charge-transfer transitions in the range 490−690 nm. With the additional catecholato donor as coligand, a second charge-transfer absorption to the diimine is present at 496 nm. The redox potential of the ferrocene unit strongly depends on the presence and type of PtL_2 moieties attached to the diimine chelate. Oxidation of the dichloroplatinum(II) complex **2** results in the formation of the expected ferrocenium cation $\mathbf{2}^{\bullet+}$. On the other hand, oxidation of the platinum(0) complex **3** in the presence of chloride labilizes the olefin coligand eventually furnishing the platinum(II) chloride complex **2** which is subsequently oxidized to $\mathbf{2}^{\bullet+}$. The first oxidation of the catecholato complex **4** is not ferrocene-centered at all but largely localized on the catecholato coligand giving a platinum-coordinated *o*-semiquinonato ligand. In the presence of chloride the *o*-semiquinonato ligand is replaced by chloride under formation of **2**. Under chloride-free conditions the

(47) Barone, V. In *Recent Advances in Computational Methods*; Chong, D. P., Ed.; World Scientific: Singapore, 1995; Part 1.

(48) Huzinaga, S.; Miguel, B. *Chem. Phys. Lett.* **1990**, *175*, 289−291.

(49) Huzinaga, S.; Klobukowski, B. *Chem. Phys. Lett.* **1993**, *212*, 260−264.

(50) The WTBS basis set was obtained from the Extensible Computational Chemistry Environment Basis Set Database, Version 02/02/06, as developed and distributed by the Molecular Science Computing Facility, Environmental and Molecular Sciences Laboratory, which is part of the Pacific Northwest Laboratory, P.O. Box 999, Richland, WA 99352, and funded by the U.S. Department of Energy. The Pacific Northwest Laboratory is a multiprogram laboratory operated by Battelle Memorial Institute of the U.S. Department of Energy under Contract DE-AC06-76RLO.

(51) Munzarová, M.; Kaupp, M. *J. Phys. Chem. A* **1999**, *103*, 9966−9983.

coordinated *o*-semiquinonato ligand in $\mathbf{4}^{\bullet+}$ has been observed by EPR spectroscopy. The unpaired electron of $\mathbf{4}^{\bullet+}$ is largely localized on the *o*-semiquinonato ligand but also interacts with the platinum nucleus and the diimine ligand. In summary, the outcome of a—at first sight—simple ferrocene-based oxidation in a complex system might well largely depend on the type of system under study as well as the oxidation conditions employed (noninnocent vs innocent oxidizing agent).

Experimental Section

General Procedures. All reactions were carried out under an atmosphere of dry argon. All solvents were dried according to standard procedures and saturated with argon prior to use. Chemicals were obtained from commercial suppliers and used without further purification. Ferrocenylpyridin-2-ylmethyleneamine[18] (Fc−N∩N′, **1**), bis(dimethyl sulfoxide)dichloroplatinum(II),[32] tris(bicyclo-[2.2.1]heptene)platinum(0),[33] and 3,6-di-*tert*-butyl[1,2]benzoquinone[34] were synthesized as reported. IR spectra were recorded on a BioRad Excalibur FTS 3000 spectrometer using cesium iodide disks. UV/vis spectra were recorded on a Perkin-Elmer Lambda 19 in 1.0 cm cells (Hellma, suprasil). Wavelengths (λ_{max}) are reported in nm, and extinction coefficients (ϵ), in M^{-1} cm^{-1}. High-resolution mass spectra (FAB+) were recorded on a JEOL JMS-700 instrument with 4-nitrobenzyl alcohol as matrix. Elemental analyses were performed by the Mikroanalytisches Laboratorium der Chemischen Institute der Universität Heidelberg. NMR spectra were obtained on a Bruker Avance DPX 200 or Avance II 400 at 25 °C. ^{1}H and ^{13}C chemical shifts are reported in ppm and calibrated to TMS on the basis of the solvent as an internal standard ($\delta = 5.31$ ppm [^{1}H] and $\delta = 53.80$ ppm [^{13}C] for dichloromethane). Assignments of ^{13}C NMR spectra were made with the aid of 2D correlation spectra. Cyclic voltammetry was performed on a Metrohm "Universal Mess- and Titriergefaess", Metrohm GC electrode RDE 628, platinum electrode, SCE electrode, and Princeton Applied Research potentiostat model 273; the substrate concentration was 1 mM in 0.1 M ^{n}Bu$_4$NPF$_6$/CH_2Cl_2. All potentials are given relative to that of SCE. Melting points were determined with a Gallenkamp capillary melting point apparatus MFB 595 010 and are not corrected. EPR spectra were recorded on a Bruker ELEXSYS E500 spectrometer (X-band). Xsophe, version 1.0.2β, was used for simulation of the spectra.

Computational Method. Density functional calculations were carried out with the Gaussian03/DFT[52] series of programs. The B3LYP formulation of density functional theory was used employing the LanL2DZ basis set.[52] All structures were characterized as minima ($N_{imag} = 0$) or first-order saddle points ($N_{imag} = 1$) by frequency analysis. Natural atomic orbital and natural bond orbital analyses were calculated using Gaussian NBO, version 3.1. Hyperfine coupling constants were obtained using the EPR-II basis set of Barone for H, C, N, and O, which is specifically optimized for the evaluation of hyperfine coupling constants.[47] For Pt the WTBS basis set[48−50] and for Fe the 6-31+g(d,p) basis set were employed, since no EPR-optimized basis sets are available for transitions metals.[50]

(Ferrocenylpyridin-2-ylmethyleneamine)dichloroplatinum-(II) [$PtCl_2$(Fc−N∩N′), 2]. A mixture of Fc−N∩N′ (**1**; 100 mg, 0.34 mmol) and bis(dimethyl sulfoxide)dichloroplatinum(0) (127 mg, 0.30 mmol) in methanol (40 mL) was stirred at 25 °C for 18 h to give a blue-green suspension. After removal of the solvent in vacuo, the residue was washed with pentane and diethyl ether, suspended in tetrahydrofuran, and precipitated with diethyl ether. Drying the residue in vacuo gave the product as a deep green solid in 69% yield (115 mg, 0.21 mmol).

IR (CsI; cm^{-1}): 1614 (m, ν_{imine}). UV/vis (CH_2Cl_2; λ_{max} (ϵ)): 263 (6355), 295 sh (4915), 341 (4005), 363 (3890), 442 (1510), 686 (835). CV (CH_2Cl_2; vs SCE): $E_{1/2} = 615$ mV (rev). Mp: 257−259 °C (262 °C dec). MS (HR-FAB+; *m*/*z* (%)): calcd for $C_{16}H_{14}{}^{35}Cl_2FeN_2{}^{196}Pt$ 555.9533, found 555.9542 (77); calcd for $C_{16}H_{14}{}^{35}ClFeN_2{}^{195}Pt$ 519.9839, found 519.9841 (44); calcd for $C_{16}H_{14}FeN_2{}^{194}Pt$ 484.0133, found 484.0085 (100). Anal. Calcd for $C_{16}H_{14}Cl_2FeN_2Pt$: C, 34.56; H, 2.54; N, 5.04. Found: C, 35.06; H, 2.81; N, 5.06.

(Ferrocenylpyridin-2-ylmethyleneamine)(η^2-fumaronitrile)-platinum(0) [Pt(Fc−N∩N′)(fn), 3]. A colorless solution of fumaronitrile (39 mg, 0.50 mmol) and tris(bicyclo[2.2.1]heptene)-platinum(0) (200 mg, 0.42 mmol) in tetrahydrofuran (20 mL) was treated with Fc−N∩N′ (**1**; 119 mg, 0.41 mmol). The deep red solution was stirred at 25 °C for 16 h. Evaporation of the solvent, washing with pentane and diethyl ether, and drying in vacuo gave the product as a deep green solid in 86% yield (199 mg, 0.35 mmol).

IR (CsI; cm^{-1}): 2203 (vs, $\nu_{CN,asym}$), 2195 (s, ν_{CNsym}), 1609 (m, ν_{imine}). UV/vis (CH_2Cl_2; λ_{max} (ϵ)): 298 (11 510), 346 (10 805), 366 sh (9360), 437 (2625), 621 (2930). CV (CH_2Cl_2; vs SCE): $E_{1/2} = 655$ mV (qrev). Mp: 274−276 °C. MS (HR-FAB+; *m*/*z* (%)): calcd for $C_{20}H_{17}FeN_4{}^{195}Pt$ 564.0450, found 564.0488 (100). Anal. Calcd for $C_{20}H_{16}FeN_4Pt$: C, 42.64; H, 2.86; N, 9.95. Found: C, 42.37; H, 3.00; N, 9.78.

(Ferrocenylpyridin-2-ylmethyleneamine)(3,6-di-*tert*-butyl-*o*-catecholato)platinum(II) [Pt(^{t}Bu$_2$Cat)(Fc−N∩N′), 4]. A solution of Fc−N∩N′ (**1**; 139 mg, 0.48 mmol), bicyclo[2.2.1]heptene (66 mg, 0.70 mmol), and tris(bicyclo[2.2.1]heptene)platinum(0) (230 mg, 0.48 mmol) in tetrahydrofuran (20 mL) was stirred at 25 °C for 4 h. After addition of 3,6-di-*tert*-butyl-1,2-benzoquinone (106 mg, 0.48 mmol), the mixture was stirred for 16 h at 25 °C. Evaporation of all volatiles, washing with pentane and diethyl ether, and drying the residue gave the product as a deep green solid in 45% yield (151 mg, 0.21 mmol).

IR (CsI; cm^{-1}): 2955 (s, $\nu_{CH-aliph.}$), 1624 (s, ν_{imine}). UV/vis (CH_2Cl_2; λ_{max} (ϵ)): 319 (15 755), 365 sh (13 550), 491 (4410), 608 (3505). CV (CH_2Cl_2; vs SCE): $E_{1/2} = 505$ mV (qrev), $E_{1/2} = 770$ mV (rev). Mp: 230−232 °C (dec). MS (HR-FAB+; *m*/*z* (%)): calcd for $C_{30}H_{35}FeN_2O_2{}^{195}Pt$ 706.1696, found 706.1797 (100); calcd for $C_{25}H_{29}FeN_2O_2{}^{195}Pt$ 640.1227, found 640.1130 (70). Anal. Calcd for $C_{30}H_{34}FeN_2O_2Pt$: C, 51.07; H, 4.86; N, 3.97. Found: C, 50.93; H, 4.96; N, 3.85.

Acknowledgment. We thank the Deutsche Forschungsgemeinschaft (Heisenberg Fellowship to K.H.) and the Graduate College 850 "Modeling of Molecular Properties" (fellowship to S.R.) for financial support.

Supporting Information Available: DFT-calculated geometries of $\mathbf{1}/\mathbf{1}^{\bullet+}$, $\mathbf{2}/\mathbf{2}^{\bullet+}$, $\mathbf{3}/\mathbf{3}^{\bullet+}$, and $\mathbf{4}/\mathbf{4}^{\bullet+}/\mathbf{4}^{2+}$ and the calculated transition states for olefin and ferrocene rotation of **3**. This material is available free of charge via the Internet at http://www.pubs.acs.org.

OM700585V

(52) Frisch, M. J.; Trucks, G. W.; Schlegel, H. B.; Scuseria, G. E.; Robb, M. A.; Cheeseman, J. R.; Montgomery, J. A., Jr.; Vreven, T.; Kudin, K. N.; Burant, J. C.; Millam, J. M.; Iyengar, S. S.; Tomasi, J.; Barone, V.; Mennucci, B.; Cossi, M.; Scalmani, G.; Rega, N.; Petersson, G. A.; Nakatsuji, H.; Hada, M.; Ehara, M.; Toyota, K.; Fukuda, R.; Hasegawa, J.; Ishida, M.; Nakajima, T.; Honda, Y.; Kitao, O.; Nakai, H.; Klene, M.; Li, X.; Knox, J. E.; Hratchian, H. P.; Cross, J. B.; Adamo, C.; Jaramillo, J.; Gomperts, R.; Stratmann, R. E.; Yazyev, O.; Austin, A. J.; Cammi, C.; Pomelli, R.; Ochterski, J. W.; Ayala, P. Y.; Morokuma, K.; Voth, G. A.; Salvador, P.; Dannenberg, J. J.; Zakrzewski, V. G.; Dapprich, S.; Daniels, A. D.; Strain, M. C.; Farkas, O.; Malick, D. K.; Rabuck, A. D.; Raghavachari, K.; Foresman, J. B.; Ortiz, J. V.; Cui, Q.; Baboul, A. G.; Clifford, S.; Cioslowski, J.; Stefanov, B. B.; Liu, G.; Liashenko, A.; Piskorz, P.; Komaromi, I.; Martin, R. L.; Fox, D. J.; Keith, T.; Al-Laham, M. A.; Peng, C. Y.; Nanayakkara, A.; Challacombe, M.; Gill, P. M. W.; Johnson, B.; Chen, W.; Wong, M. W.; Gonzalez, C.; Pople, J. A. *Gaussian 03*, revision B.03; Gaussian, Inc.: Pittsburgh, PA, 2003.